Available online at www.sciencedirect.com
SCIENCE DIRECT®
Nuclear Engineering and Design 235 (2005) 1139–1148
Nuclear Engineering and Design
www.elsevier.com/locate/nucengdes

Study of countercurrent flow limitation in a horizontal pipe connected to an inclined one

Moysés Alberto Navarro *

Comissão Nacional da Energia Nuclear (CNEN), Centro de Desenvolvimento da Tecnologia Nuclear (CDTN), Rua Prof. Mario Werneck s/n, Cidade Universitária, Pampulha, 30123-970 Belo Horizonte, Brazil

Received 13 January 2005; received in revised form 14 January 2005; accepted 16 February 2005

Abstract

Experiments with air and water in small hot leg reproductions were carried out aiming to acquire a better understanding of the countercurrent flow limitation (CCFL) in this geometry. The effects of various geometrical parameters of the test section and of the inlet water flow rate on the onset of flooding, on the partial delivery of water and on the zero liquid penetration were investigated. It was observed that while the onset of flooding is affected by the inlet water flow rate, the zero liquid penetration is independent of this flow rate. The results with partial delivery showed that, for a fixed air velocity, an increase in the horizontal length, or in the inclined length, of the flow channel leads to an increase of the water carried over by the air. On the other hand, in pipes with larger diameters the drag of the water is smaller. The experimental results showed small differences in the results for tests with inclination of the riser lower than 90°. For an inclination equal to 90°, the water carried by the air tends to be lower than in the others angles for a fixed air velocity. The study led also to a new correlation for the flooding.

1. Introduction

The countercurrent flow limitation (CCFL), or flooding, represents a condition in which a gas flow establishes a control on the liquid flow in the opposite direction. The phenomenon plays an important role in several equipments of the chemical and mechanical industries (reflux condensers, packed columns, heat pipes, etc.) and has also been receiving special attention of the nuclear industry due to its influence on the thermo-hydraulic behavior of pressurized water reactors (PWR) during a loss of coolant accident (LOCA). In the blowdown phase of a large break, the Emergency Core Coolant System (ECCS) injects cold water to reduce the temperature of fuel elements that increases quickly due to the radioactive decay of the fission products. The penetration of this water in the primary circuit of the reactor can be limited by the steam flow in the opposite direction at some critical locations, such as in the tubes of the steam generator, in the downcomer and in the fuel element top nozzle (tie plate). In a small break accident the steam flowing from the core condenses in the steam generator tubes. This situation corresponds

* Tel.: +55 31 34993138; fax: +55 31 34993411.
E-mail address: navarro@cdtn.br.

0029-5493/$ – see front matter © 2005 Elsevier B.V. All rights reserved.
doi:10.1016/j.nucengdes.2005.02.010

Nomenclature

C	constant in the Wallis' correlation
D	diameter (m)
g	gravitational acceleration (m/s^2)
H	water head (m)
j	superficial velocity (m/s)
j^*	dimensionless superficial velocity
L	length (m)
M	constant in the Wallis' correlation
P	pressure (N/m^2)
q_m	mass flow rate (kg/s)
s	standard error
T	temperature (K)
t	time (s)

Greek letters

α	void fraction
θ	angle of the inclined pipe (rad, °)
ρ	density (kg/m^3)

Subscripts

g	gas, air
gc	gas calculated
ge	gas experimental
go	gas-onset of flooding
gt	gas-onset of total carryover (zero liquid penetration)
H	horizontal
I	inclined
l	liquid
li	liquid-injected

to the reflux-condensing mode. The condensed liquid falls through the reactor hot leg where its flow may be limited by the steam coming from the upper plenum.

Initially, the studies The CCFL phenomenon were focused on vertical, horizontal and annular channels and less on channels with flow through perforated plates. The geometry constituted of a horizontal tube connected to an inclined riser, as a PWR hot leg, has been receiving attention more recently.

In order to better understand the influences of some geometric parameters on the behavior of the CCFL in the hot leg geometry, a series of experiments was carried out in scaled test sections with this geometric form. In addition, a new correlation that considers the effects of the geometric characteristics of the flow channel on the flooding is proposed.

2. Previous works

The first experimental studies of flooding were accomplished in vertical single tube where, in a basic experiment, the liquid was injected either through the upper extremity or through a porous membrane in the wall, and the feeding of gas was done either through a lower plenum or through a nozzle in the bottom exit. The principal goals of these experiments are the determination of the gas velocity necessary to start the liquid dragging process (onset of flooding) and of the gas velocity at the initial moment in which the liquid is totally carried up (or zero liquid penetration limit). The studies conducted by Wallis (1961) turned into reference for many researchers. He correlated his experimental data, obtained in circular vertical sections, with the expression:

$$(j_g^*)^{1/2} + M(j_l^*)^{1/2} = C \quad (1)$$

where j_l^* and j_g^* are the dimensionless parameters:

$$j_k^* = \frac{\rho_k^{1/2} j_k}{[gL(\rho_l - \rho_g)]^{1/2}} \quad (2)$$

and j_k is the superficial velocity of the k-phase (k = l (liquid); k = g (gas)), ρ_k the respective densities, L the characteristic length of the flow channel (L = diameter for circular sections) and g is the gravitational constant. In this model, M and C are constants, which are adjusted to the experimental results. In the Wallis experiments M assumed the values from 0.8 to 1.0 and $0.7 < C < 1$. Since then, this correlation has been frequently used by other investigators to correlate experimental results obtained not only in vertical pipes but also in other geometric forms and the constants assumed the ranges: $0.6 < M < 1.2$ and $0.3 < C < 1$.

The most important investigations of the flooding in a flow path constituted of an horizontal tube connected to an inclined riser are listed in Table 1. The studies in hot leg geometry demonstrate some inconsistencies in the extrapolation of results obtained in small scale test sections to the real situation. It was also observed

Table 1
Experimental studies of the countercurrent flow limitation in horizontal and inclined pipes connected by a bend

Experiment	L_H (m)	L_I (m)	θ (°)	D (m)	Exp. correlation
Richter et al. (1978)	0.9144	–	45	0.2032	Wallis; $C = 0.7$; $M = 1$
Krolewski (1980)	0.584	0.305	45; 90	0.0508	Wallis; $C = 0.53$; $M = 0.78$ ($\theta = 45°$)
Ohnuki (1986)	0.01–0.4	0.038–0.6	40; 45	0.026; 0.051; 0.076	Wallis; $C = \ln\{(L_H/D)(1/L_I)\}^{-0.066} + 0.88$; $M = 0.75$
Siddiqui et al. (1986)	$24D < L_H < 95D$	–	90	0.0365–0.047	Wallis; $(j^*_{gt})^{1/2} = 0.45$
Ohnuki et al. (1988)	0.26	0.06	50	0.0254	Wallis; $C = \ln\{(L_H/D)(1/L_I)\}^{-0.066} + 0.88$; $M = 0.75$
Kawaji et al. (1989)	0.1; 2.54	–	90	0.051	–
UPTF (Weiss et al., 1992)	7.197	1.27	50	0.75	Wallis; $C \cong 0.7$; $M \cong 1$
MHYRESA (Geffraye et al., 1995)	2.645; 2.473	1.06; 1.194	50	0.352; 0.075	$(j^*_{gt})^{1/2} = 0.52$; $(j^*_{gt})^{1/2} = 0.61$
Wongwises (1996)	0.557–2.816	∼1.26	50; 75; 90	0.064	–
Chun et al. (1999)	0.7–3.388	0.623; 0.648	35	0.04; 0.08	Wallis; $C = 0.603–0.00234(L_H/D)$; $M = 0.397$

that the mechanisms which define the onset of flooding in this geometry differ of those observed in other geometric forms. The influences of some dimensional parameters, such as inclination of the bend (θ), horizontal and inclined lengths (L_H; L_I), diameter (D) or of the experimental procedure, on the behavior of the flooding are not well understood yet. This paper presents results of experiments in which these influences were appraised and in this way it may contribute to a better understanding of the phenomenon.

3. Experimental set-up and procedure

Fig. 1 shows a schematic diagram of the experimental system used in the study of CCFL. Water and air, at room temperature and atmospheric pressure, are the working fluids.

In a typical experiment, the water from the reservoir (ST) is pumped to the upper tank (UT) from where it precipitates by gravity through the test section to the lower tank (LT). The air injected in the lower tank flows in countercurrent through the test section to the upper tank and after that is released to the atmosphere. After the onset of flooding, a portion of the water is impeded by the air of precipitating to the lower tank and accumulates in the right side of the upper tank until a level defined by a separator plate is reached (H). The flow rates of the falling water and of the carried water are measured through the rate of level rise in tanks FT and CT, respectively. These flow rates and the injected water flow rate, obtained by pressure drop in an orifice plate, make it possible to perform the water mass balance. Pressure drop in orifice plates are also used to measure the air flow rates.

The test section, as well as the laterals of the upper and lower tanks, were made in acrylic to permit visual observation of the countercurrent flow. Fittings were developed to allow a fast connection between the tanks and the horizontal and inclined tubes whose lengths can be varied during the experiments. The connections between the tubes and the bend were also designed in such a way that the parts can be changed quickly.

Besides the flow rates of the fluids were also measured the fluid temperatures, the pressure in the upper tank, the differential pressure between the upper and the lower tanks and the level of the water (void fraction) in three positions along the horizontal part of the test section: 0.01 m from the bend (α_1), 0.01 m from the connection with the lower tank (α_3) and in the half distance between these extremities (α_2). These measurements were done using attenuation of gamma-radiation in the two-phase flow (Am241, ∼60 keV).

The analog output signals from the gauges were transmitted to a Data Acquisition System (DAS) which processed and displayed on-line the evolution of the experimental parameters. Averages of all experimental parameters were evaluated during 1 s (100 data acquisitions) for each air flow rate level and these values were then stored for subsequent analysis.

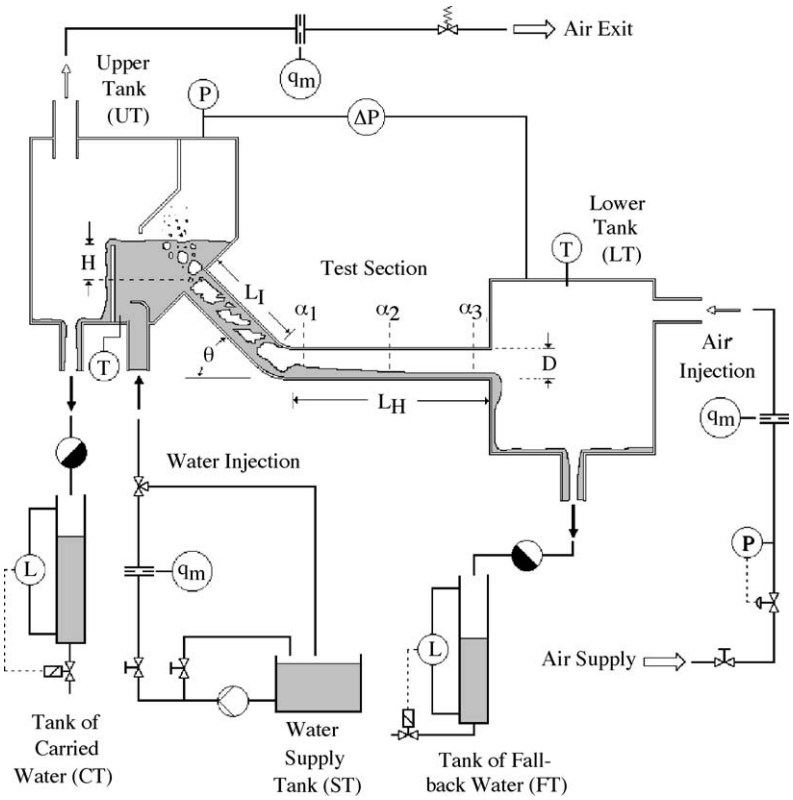

Fig. 1. Schematic diagram of experimental apparatus.

The experiment matrix includes various water and air flow rates for each test section configuration (L_H, L_I, D, θ, H) showed in Table 2. The table also shows the ranges of the superficial velocities of the injected and precipitated water (j_{li}, j_l) and of the air (j_g).

Table 2
Range of the experimental parameters

Parameter	Experimental values		
D (m)	0.054	0.036	0.044
θ (°)	30; 50; 70; 90	50	50
H (m)	0; 0.01; 0.02; 0.04; 0.085; 0.13	0.04	0.04
L_H (m)	0.10; 0.30; 0.50[a]; 0.80	0.35[a]; 0.80	0.42[a]; 0.80
L_I (m)	0.10; 0.30; 0.50	0.10; 0.35	0.10
j_{li} (m/s)	0.022–0.22 (±0.004)		
j_g (m/s)	0.6–8.0 (±0.01)		
j_l (m/s)[b]	0–0.22 (±0.004)		

[a] L_H/D close to the PWR ratio.
[b] Precipitated water.

An experiment was initiated with the establishment of a specified water flow rate and soon afterwards a low air flow rate. The air flow rate was increased by small increments, until the beginning of the water drag by the air (onset of flooding) and afterwards until the water was impeded of precipitating in the lower tank (zero liquid precipitation). Finally, the air flow rate was reduced, also gradually, until the total precipitation of the water again (partial delivery).

4. Results

4.1. Typical behavior

Fig. 2 shows the superficial velocity behavior of the downward water as a function of the superficial air velocity for a particular configuration of the test section. A similar qualitative behavior was obtained in the other configurations. The experimental results obtained with

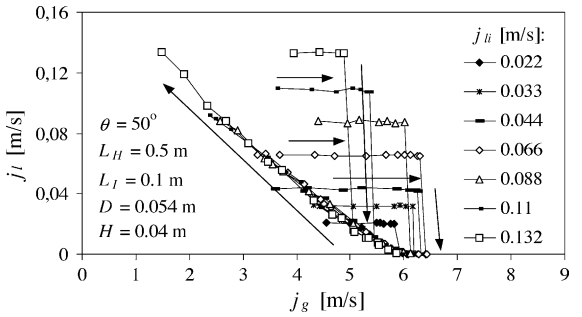

Fig. 2. Velocity diagram for different injected water superficial velocities.

different injected superficial water velocities are represented in Fig. 2. It can be observed in the figure that, for any fixed j_{li}, during the increasing air injection phase, all the injected water precipitates to lower tank until the beginning of the dragging process (onset of flooding). This is characterized by the abrupt drop in the superficial velocity of the downward water. After this point, depending on injected superficial water velocity, the precipitate quantity can be reduced either to a characteristic tendency (flooding curve) until the total water carry-up for $j_{li} > 0.088$ m/s (zero liquid penetration: $j_g \cong 5.9$ m/s) or direct to zero water precipitation for $j_{li} < 0.088$ m/s. The similarity among the curves after the onset of flooding and during the air flow reducing demonstrates that the injection water velocity does not influence the established limitation process (partial delivery).

The air velocities required to onset of flooding as function of the injected water velocities are represented in terms of Wallis dimensionless parameters $((j_{li}^*)^{1/2} \times (j_{go}^*)^{1/2})$ in the diagram of Fig. 3, for the same test section considered previously. Depending on

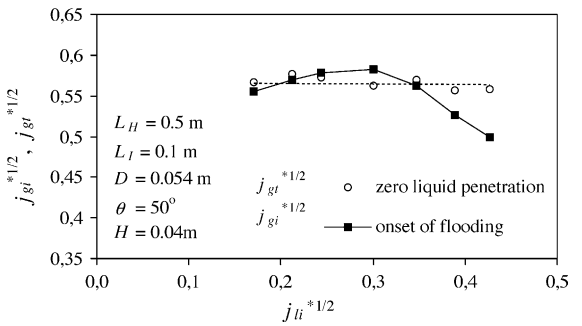

Fig. 3. Onset of flooding as a function of the water injection rates.

the injected superficial water velocity, two different tendencies for the onset of flooding can be observed.

In the range $0.17 < (j_{li}^*)^{1/2} < 0.3$, which corresponds to 0.022 m/s $< j_{li} < 0.066$ m/s, the onset of flooding occurs in the lower extremity of the test section (in the connection with the lower tank). For very low air velocities the injected water falls initially far from the vertical wall of the lower tank. With the increase of the superficial air velocity, a small slug is formed at the horizontal pipe extremity and from this air–water interface water droplets are carried to the upper wall of the pipe. When the flooding point is reached, the slug is already larger and is pushed quickly upwards. In its displacement, the slug becomes bigger as it approaches the bend. Near the bend the slug reaches near the superior surface of the pipe, and momentarily blocks the water precipitation. In a churned way, the water accumulates in the inclined pipe and soon afterwards in the upper tank. From this moment, there is no precipitation of water in the lower tank and the injected water accumulates in the upper tank until the H level, defined by the separator plate. The flow pattern is stratified roll wavy in the horizontal pipe, with a water level gradient decreasing from the bend to the lower exit, and churned wobbly in the inclined pipe. For this injected water range, an increase in the injected superficial water velocity leads to an increase of the falling water velocity in the lower tank and this demands higher air velocity to onset of flooding.

If the injected water superficial velocity approximates 0.066 m/s ($(j_{li}^*)^{1/2} \leq 0.3$), the open cross section for the air flow in the upper extremity of the test section (in the connection with the upper tank) becomes smaller causing a new dragging process at this extremity. This process occurs almost simultaneously to the onset of flooding in the lower exit, and remains for $j_{li} = 0.088$ m/s. The injected water accumulates in the upper tank and no water precipitation to the lower tank occurs. A partial precipitation of the water after the onset of flooding is observed for $j_{li} > 0.088$ m/s. In the range 0.066 m/s $< j_{li} < 0.132$ m/s, an increase in the injected superficial water velocity reduces even more the area to the air flow and, consequently, the air velocity to begin the upper dragging. The amount of falling water and the air velocity to onset of flooding in the lower extremity are also reduced.

Fig. 3 shows also that the zero liquid penetration points (or return to the precipitation in the phase with

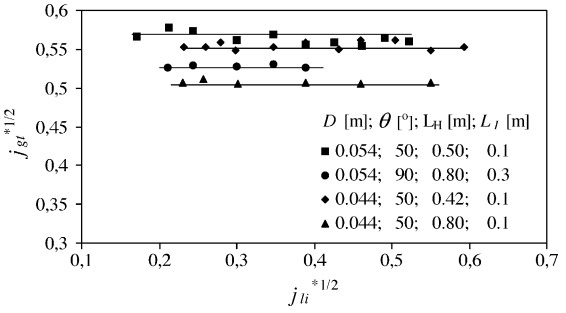

Fig. 4. Zero liquid penetration as function of the water injection rates.

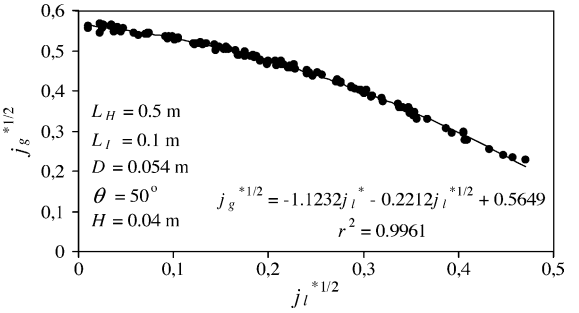

Fig. 6. Flooding diagram for different water injection rates.

air reduction) are practically independent of the injected superficial water velocity, $(j_{li}^*)^{1/2}$. Fig. 4 confirms, however, that these points are influenced by the geometrical parameters of the test section.

As show in Fig. 5 the two tendencies shown for $\theta = 50^\circ$ were observed also in other test section configuration with $\theta = 30^\circ$ and 70°. With these inclinations no hydraulic jump in the horizontal pipe of the test section as result from the change of a super-critical flow to a sub-critical flow was observed.

The hydraulic jump was only observed in the test configuration with $\theta = 90^\circ$ at low inlet water flow rates. For this situation, the hydraulic jump was observed thin and near to the bend, at low injected water flow rates, and bigger and far from the bend at higher inlet water flow rates. At the flooding point, drops of water are extracted from the crest of the hydraulic jump, where the air velocity is higher, and carried up by the air. Bigger hydraulic jumps, obtained with higher injected water flow rates, demand lower air superficial velocities to onset of flooding. This explains the decreasing tendency observed in Fig. 5 for $\theta = 90^\circ$ and $(j_{li}^*)^{1/2} < 0.2$.

Fig. 6 shows the flooding curve for the same geometric configuration presented in Fig. 3. The data correspond to the partial delivery phase obtained with the reduction on the injected air flow rate, from the zero liquid penetration to total water precipitation, for all the injected water flow rates. A perfect linear relationship between the Wallis parameters as defined by Eq. (1) is not observed for this geometric form.

Fig. 7 shows the behavior of the pressure drop between the upper and lower tanks during the increase (A–D) and the decrease (D–F) of the air flow rate, for the injected superficial water velocity 0.132 m/s. The abrupt increase B–C corresponds to the onset of flooding and point F represents the return to total precipitation.

The decreasing profile of the interface during the partial delivery phase (C–D–E) is illustrated in Fig. 8 by the measurements of void fractions in three positions along the horizontal pipe. All the water injection velocities are represented in the figure.

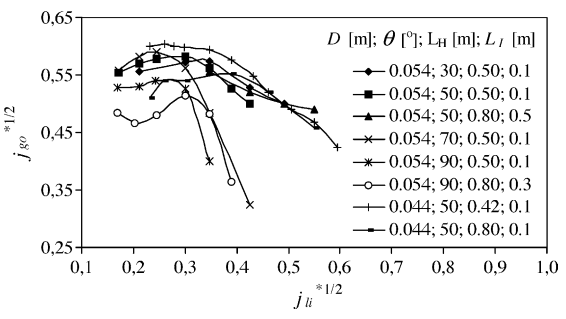

Fig. 5. Onset of flooding for different geometrical parameters of the test section.

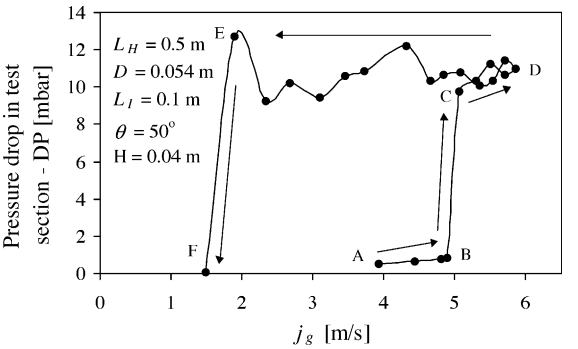

Fig. 7. Pressure drop in the test section for $j_{li} = 0.132$ m/s.

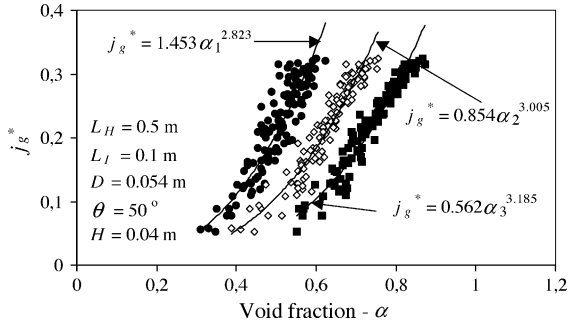

Fig. 8. Void fraction along the horizontal pipe of the test section during the partial delivery.

4.2. Effect of geometric parameters on the partial delivery

The influences of dimensional characteristics (L_H, L_I, D, θ) of the test section and of the injected water flow rate on the onset of flooding, were also verified in the experiments performed by Wongwises (1996), Kawaji et al. (1989) and Chun et al. (1999). However, in the present study it was observed that although the limitation process with partial delivery also depends on the geometric characteristics of the test section it is not affected by the injected water flow rate and presents a characteristic behavior as shown in Fig. 6.

Figs. 9–14 show the influences of the geometric parameters L_H, L_I, D, H and θ on the partial delivery curve. The results are displayed in terms of the Wallis parameters $((j_l^*)^{1/2} \times (j_g^*)^{1/2})$.

Fig. 9 shows that the air velocity necessary to begin the total water dragging (zero liquid penetration point) decreases with longer L_H. It can still be observed in the figure that, for a fixed air velocity, the velocity of the precipitated water also decreases with the increase of the horizontal length.

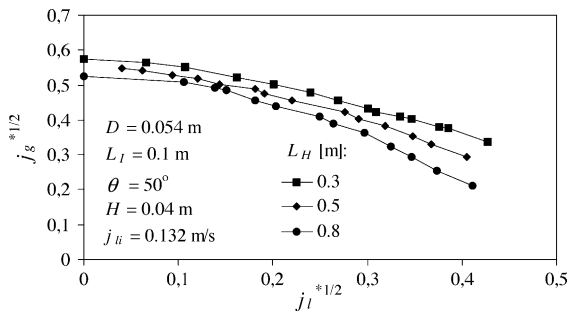

Fig. 9. Effect of the horizontal length of the test section on the partial delivery.

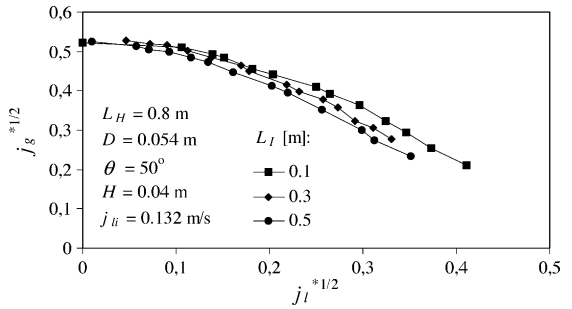

Fig. 10. Effect of the inclined length of the test section on the partial delivery.

Fig. 10 shows that an increase in the inclined length of the test section produces, for a fixed air velocity, a small reduction on the water precipitation and almost any influence on the null penetration point.

The influence of the diameter of the flow channel on the flooding curve is showed in Fig. 11. Larger diameters produces smaller drag of the water. Fig. 12

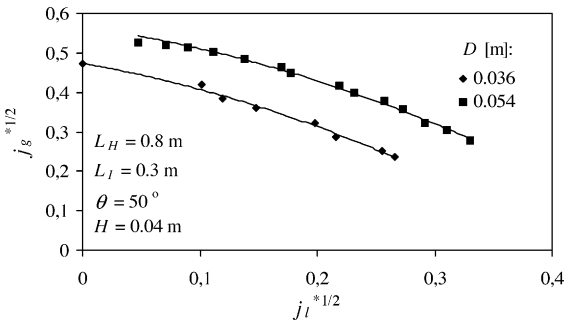

Fig. 11. Effect of the diameter of the test section on the partial delivery.

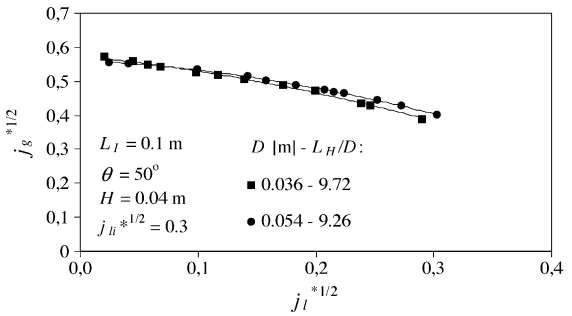

Fig. 12. Effect of the test section L_H/D ratio on the partial delivery.

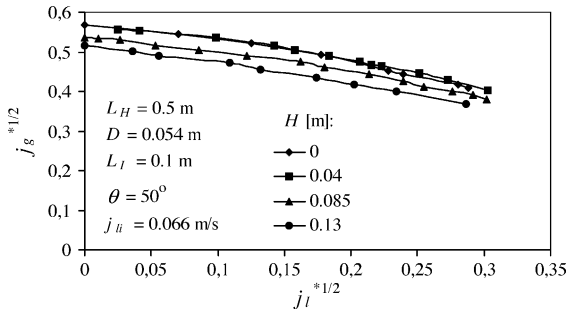

Fig. 13. Effect of the water head above the upper exit of the test section on the partial delivery.

shows that, for very similar L_H/D ratios, the difference between the flooding curves is also minimal.

The effect of the water head, H, above the upper extremity of the test section on the flooding curve is shown in Fig. 13. Almost no difference could be observed between the curves that were obtained with $H < 4$ cm. However, for $H > 4$ cm, an increase in the liquid head induces to a reduction of the air velocity for zero liquid penetration and, for a fixed air velocity, to a reduction of the water precipitation.

Fig. 14 shows a slight reduction on air velocity to the zero liquid penetration with the increase in the slope of the inclined pipe of the test section. Small differences exist among curves with $\theta = 30°$, 50° and 70°. The increase of θ to 90° produces lower precipitation compared to the other studied slopes.

4.3. Empirical correlation

Based on the effects of the dimensional parameters on partial delivery, concisely presented in the previous sections, an empiric model for the flooding curve was adjusted. It was obtained by multiple regression in 888 experimental points with the following ranges of dimensional parameters: $1.85 < L_I/D < 9.25$; $1.85 < L_H/D < 22.2$; $30° < \theta < 90°$. The basic formula for the model is a quadratic equation with the Wallis parameters $(j_g^*)^{1/2}$ and $(j_l^*)^{1/2}$:

$$(j_g^*)^{1/2} = F_0 + F_1(j_l^*)^{1/2} + F_2 j_l^* \tag{3}$$

where the functions F_0, F_1 and F_2 are expressed in terms of the dimensional parameters:

$$F_0 = -0.04722\theta - 1.5649 \times 10^{-4}\left(\frac{L_H}{D}\right)^2 - 0.16539\left(\frac{H + D\cos\theta/2}{D}\right)^{0.2} + 0.78375 \tag{4}$$

$$F_1 = 0.507\theta^{0.2} - 0.26015\left(\frac{L_H}{D}\right)^{0.46} - 0.00121\left(\frac{L_I}{D}\right)^{1.2} \tag{5}$$

$$F_2 = -1.03549\theta - 0.5881\left(\frac{L_H}{D}\right)^{0.3} + 0.20163\left(\frac{L_H\theta}{D}\right)^{0.7} \tag{6}$$

where θ should be supplied in radian and the other dimensions in m.

Fig. 15 compares the $(j_g^*)^{1/2}$ calculated by Eq. (3) with the $(j_g^*)^{1/2}$ obtained experimentally. With respect

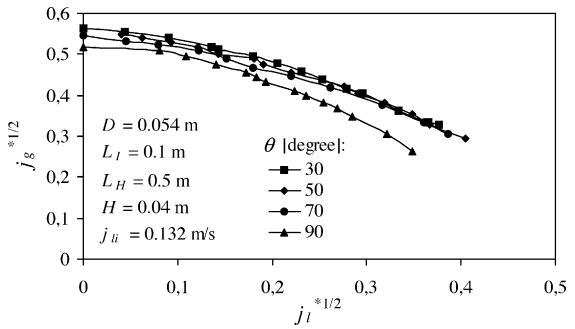

Fig. 14. Effect of the inclination θ of the test section on the partial delivery.

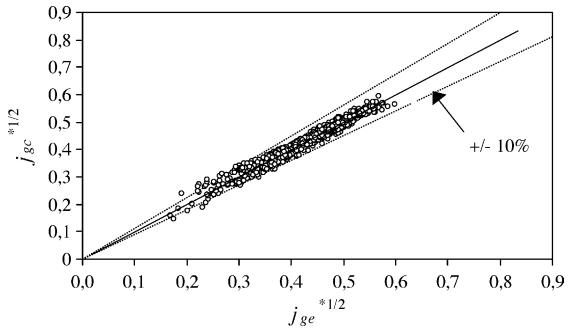

Fig. 15. Comparison of the present model with the experimental data.

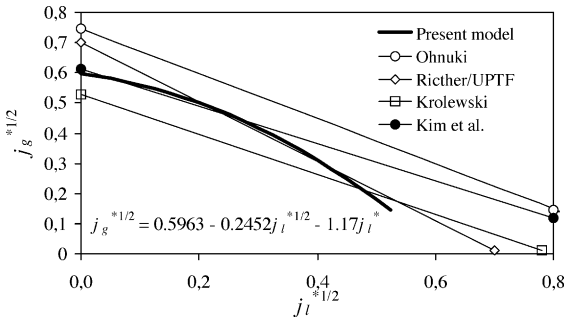

Fig. 16. Comparison of the present model with other models applied to the dimensions of a PWR hot leg.

to the experimental data, the model presents a error 2.9%, defined as:

$$s = \frac{1}{n} \sum \left| \frac{(j_{ge}^*)^{1/2} - (j_{gc}^*)^{1/2}}{(j_{gc}^*)^{1/2}} \right| 100 \qquad (7)$$

The developed correlation with $H = 0$ m when applied to the dimensions of a PWR hot leg can be reduced to a simpler model:

$$(j_g^*)^{1/2} = 0.5963 - 0.2452(j_l^*)^{1/2} - 1.17 j_l^* \qquad (8)$$

This model is compared with other correlations in Fig. 16. The Wallis correlation (Eq. (1)) adjusted to experimental results obtained in UPTF (Weiss et al., 1992) ($M = 1$, $C = 0.7$) is used as reference in these comparisons. The same correlation was obtained by Richter et al. (1978) in a intermediate scale test section. The correlation obtained in a small test section by Ohnuki (1986) (see Table 1) overpredicts the UPTF results and, on the other hand, the Krolewski (1980) correlation underpredicts the UPTF results. It can be observed that, for $(j_g^*)^{1/2} < 0.5$, the present model agrees well with the model adjusted to the UPTF results; however, for $(j_g^*)^{1/2} > 0.5$, the water precipitation computed by the present model is slightly smaller. Fig. 16 also shows the recent model, presented by Kim et al. (2001), adjusted by regression through 356 experimental points of different researchers:

$$(j_g^*)^{1/2} = 0.635 - 0.00254 \left(\frac{L_H}{D} \right) - 0.614 (j_l^*)^{1/2} \qquad (9)$$

5. Conclusions

The air–water countercurrent flow limitation was investigated in the geometry of the hot legs of PWRs. In this study, it was verified that the onset of flooding does not depend only on the dimensional characteristics of the test section but also on the injected water flow rate. Depending on this flow rate different mechanisms lead to onset of flooding, which can occur in different positions of the test section: at the horizontal pipe, close to the bend, for low flow rate, due to the formation of a hydraulic jump; at the lower end, for intermediate flow rates, with the formation of a slug in this position, and at the upper extremity, due to the area reduction to the air flow with higher injected flow rates. The limitation phase with partial delivery, however, does not depend on the injected water flow rate and is only influenced by the dimensional characteristics of the test section. From the analysis of the influences of the geometric characteristics of the test section on the flooding curve with partial delivery, the following conclusions were obtained: for a fixed air velocity, an increase in the horizontal length or in the inclined length of the flow channel provokes an increase in the water carried out by the air, while an increase of the diameter leads to a decrease of the carried water. Little difference was observed among the curves with inclinations lower than 90°. For this inclination, however, the carried water tends to be larger than in others angles for a fixed air velocity.

A new flooding correlation was derived by regression through the experimental points in the dimensional ranges: $1.85 < L_I/D < 9.25$; $1.85 < L_H/D < 22.2$; $30° < \theta < 90°$. Although the developed correlation had been obtained from experiments in small scale reproductions of hot legs of PWRs, for $(j_g^*)^{1/2} < 0.5$ the model presents a reasonable agreement with experimental results obtained in the real scale of a PWR, and for $j_g^{*1/2} > 0.45$ it agrees well with the model obtained by Kim et al. (2001) by regression through experimental results of several researchers.

References

Chun, M.H., No, H.C., Kang, S.K., Chu, I.C., 1999. Countercurrent flow limitation in a horizontal pipe connected to an inclined riser. Trans. ANS 81, 340–341.

Geffraye, G., Bazin, P., Pichon, P., Bengaouer, A., 1995. CCFL in hot legs and steam generators and its prediction with the

CATHARE Code. In: Proceedings of the Seventh NURETH, Saratoga Springs, NY.

Kawaji, M., Thomson, L.A., Krishnan, V.S., 1989. Countercurrent flooding in an elbow between a vertical pipe and a downwardly inclined pipe. In: Proceedings of the Fourth NURETH, Karlsruhe, Germany, 20–27.

Kim, H.T., No, H.C., Ha, S.J., Ahn, N.S., Bang, Y.S., 2001. Assessment of RELAP5/MOD3.2.2γ Against Flooding Database in Horizontal-to-Inclined Pipes. U. S. Nuclear Regulatory Commission Report NUREG/IA-0203.

Krolewski, S.M., 1980. Flooding Limit in a Simulated Nuclear Reactor Hot Leg. BS Thesis. Massachusetts Institute of Technology, Cambridge, MA.

Ohnuki, A., 1986. Experimental study of counter-current two-phase flow in horizontal tube connected to inclined riser. J. Nucl. Sci. Technol. 23, 219–232.

Ohnuki, A., Adachi, H., Murao, Y., 1988. Scale on countercurrent gas–liquid flow in a horizontal tube connected to an inclined riser. Nucl. Eng. Des. 107, 283–294.

Richter, H.J., Wallis, G.B., Carter, K.H., Murphy, S.L., 1978. Deentrainment and Countercurrent Air–Water Flow in a Model PWR Hot Leg. U. S. Nuclear Regulatory Commission Report NRC-0193-9.

Siddiqui, H., Ardron, K.H., Banerjee, S., 1986. Flooding in an elbow between a vertical and a horizontal or near-horizontal pipe. Part I. Experiments. Int. J. Multiphase Flow 12, 531–541.

Wallis, G.B., 1961. Flooding Velocities for Air and Water in Vertical Tubes. UKAEA Report AEEW-R123.

Weiss, P., Emmerling, R., Hertlein, R., Liebert, J., 1992. Two-phase flow experiments in full-scale to extend knowledge of PWR LOCA thermal–hydraulics. In: ANS Proceedings of the National Heat Transfer Conference, vol. 6, San Diego, California, pp. 268–282.

Wongwises, S., 1996. Two-phase countercurrent flow in a model of a pressurized water reactor hot leg. Nucl. Eng. Des. 166, 121–133.